

Custom-designed high-density conformal planar multielectrode arrays for brain slice electrophysiology

Ghassan Gholmieh^{a,*}, Walid Soussou^{b,1}, Martin Han^{a,c,1}, Ashish Ahuja^c, Min-Chi Hsiao^a, Dong Song^a, Armand R. Tanguay Jr.^{a,b,c}, Theodore W. Berger^{a,b}

^a Department of Biomedical Engineering, University of Southern California, Los Angeles, CA 90089-1451, USA

^b Neuroscience Program, University of Southern California, Los Angeles, CA 90089-2520, USA

^c Department of Electrical Engineering, University of Southern California, Los Angeles, CA 90089, USA

Received 10 November 2004; received in revised form 20 July 2005; accepted 30 August 2005

Abstract

Multielectrode arrays have enabled electrophysiological experiments exploring spatio-temporal dynamics previously unattainable with single electrode recordings. The finite number of electrodes in planar MEAs (pMEAs), however, imposes a trade-off between the spatial resolution and the recording area. This limitation was circumvented in this paper through the custom design of experiment-specific tissue-conformal high-density pMEAs (cMEAs). Four configurations were presented as examples of cMEAs designed for specific stimulation and recording experiments in acute hippocampal slices. These cMEAs conformed in designs to the slice cytoarchitecture whereas their high-density provided high spatial resolution for selective stimulation of afferent pathways and current source density (CSD) analysis. The cMEAs have 50 or 60 μm center-to-center inter-electrode distances and were manufactured on glass substrates by photolithographically defining ITO leads, insulating them with silicon nitride and SU-8 2000 epoxy-based photoresist and coating the etched electrode tips with gold or platinum. The ability of these cMEAs to stimulate and record electrophysiological activity was demonstrated by recording monosynaptic, disynaptic, and trisynaptic field potentials. The conformal designs also facilitated the selection of the optimal electrode locations for stimulation of specific afferent pathways (Schaffer collaterals; medial versus lateral perforant path) and recording the corresponding responses. In addition, the high-density of the arrays enabled CSD analysis of laminar profiles obtained through sequential stimulation along the CA1 pyramidal tree.

© 2005 Elsevier B.V. All rights reserved.

Keywords: Planar; Conformal; High-density; Multielectrode array; Current source density analysis; Hippocampal slice

1. Introduction

The capability of simultaneously recording electrical activity at multiple sites in vitro has enabled investigations of neuronal network dynamics previously not possible with single electrode recordings (Droge et al., 1986; Singer, 2000; Soussou et al., in press; Warland et al., 1997). Planar multielectrode arrays (pMEAs) present one currently available technology to record from multiple neurons simultaneously in vitro (Duport et al., 1999; Egert et al., 1998; Gross and Schwalm, 1994; Jahnsen et al., 1999; Jimbo and Robinson, 2000; Novak and

Wheeler, 1988; Oka et al., 1999; Stoppini et al., 1997). The distribution of pMEA electrodes captures the spatio-temporal dynamics of neuronal activity, while their transparent conductive leads permit microscopic visualization of the relative position of the tissue with respect to electrodes. Planar MEA electrodes can be used for both recording and stimulation, thereby providing self-contained sterile systems with no need for external electrodes (Gross et al., 1993; Novak and Wheeler, 1988).

Low cost of photolithographic fabrication coupled with advances in signal acquisition hardware and fast computers with large data storage, has led several groups to independently develop their own pMEAs. These investigators developed thin-film pMEAs in a variety of configurations to monitor extracellular electrophysiological activity in acute and cultured slices from different brain areas: retina (Grumet et al., 2000; Meister et al., 1994), spinal cord (Borkholder et al.,

* Corresponding author at: University of Southern California, 3614 Watts Way, HNB 403, Los Angeles, CA 90089-2520, USA. Tel.: +1 213 740 8061; fax: +1 213 740 5687; mobile: +3109770589.

E-mail address: gholmieh@usc.edu (G. Gholmieh).

¹ These authors contributed equally to this paper.

1997), and hippocampus (Boppart et al., 1992; Egert et al., 1998; Heuschkel et al., 2002; Novak and Wheeler, 1988; Oka et al., 1999; Thiebaud et al., 1999). In addition, several commercial planar multielectrode recording systems have recently become available such as MEA60 from Multi Channel Systems, Reutlingen, Germany and MED64 from Panasonic, CA, USA.

The advantages offered by pMEAs over traditional extracellular pulled-glass or sharp-wire electrodes depend on the number of electrodes, which is limited by current technological constraints, such as electrode and lead overcrowding, cross-talk, connector design, and data acquisition. These limitations create a trade-off between spatial sampling resolution and coverage area, preventing stimulation and recording from every location of a tissue preparation. Most of these currently available pMEAs have electrodes distributed in square matrix configurations with relatively large inter-electrode spacing (greater or equal to $100\ \mu\text{m}$). Since neural cytoarchitecture changes dramatically in the spatial domain in a non-symmetrical fashion, these low-density geometrically regular electrode arrangements do not provide the necessary resolution for selectively stimulating afferent pathways or flexibility in recording from small subregions. Furthermore, the low electrode density does not permit adequate current source density (CSD) analysis (Freeman and Nicholson, 1975; Nicholson and Freeman, 1975; Nicholson and Llinas, 1975; Wheeler and Novak, 1986). Therefore, there is a need to create tissue-specific high-density cMEAs that conform to the cytoarchitecture of the nervous tissue of interest. This paper resolves this compromise by describing custom pMEAs (cMEAs) that have a high-density of electrodes in tissue-conformal configurations for specific experimental applications.

This study describes methodology for designing, fabricating and using such conformal high-density cMEAs, and presents four examples of such pMEAs suited for CSD analysis, three of which are conformally mapped to hippocampal slice cytoarchitecture. The conformality refers to electrode distributions that correspond to the organization of intrinsic hippocampal circuitry. Stimulating electrodes are thus concentrated under afferent fibers or presynaptic cells, while recording electrodes are arranged under postsynaptic dendrites and somas. These layouts were designed for *in vitro* stimulation and recording from different hippocampal subregions (Fig. 1): cMEA#1 is a 3×20 rectangular array created for CSD analysis, and is well suited for electrophysiological investigations of the pyramidal and granular cells of the hippocampus, since these cells are densely packed into columns of parallel dendrites; cMEA#2 was designed to stimulate Schaffer Collateral (SchC) afferents to CA1 and records their responses; cMEA#3 design was intended for the stimulation of perforant path (PP) fibers in order to excite the dentate gyrus (DG) and the CA3 area; cMEA#4 was designed to stimulate PP and record DG, CA3 and CA1 responses in order to trigger trisynaptic responses.

Conformal topographical mapping and high electrode density enabled fine control and easy optimization of stimulation and recording sites. Large signal-to-noise ratios ($>10:1$) and high spatial density of electrodes has enabled CSD analysis of

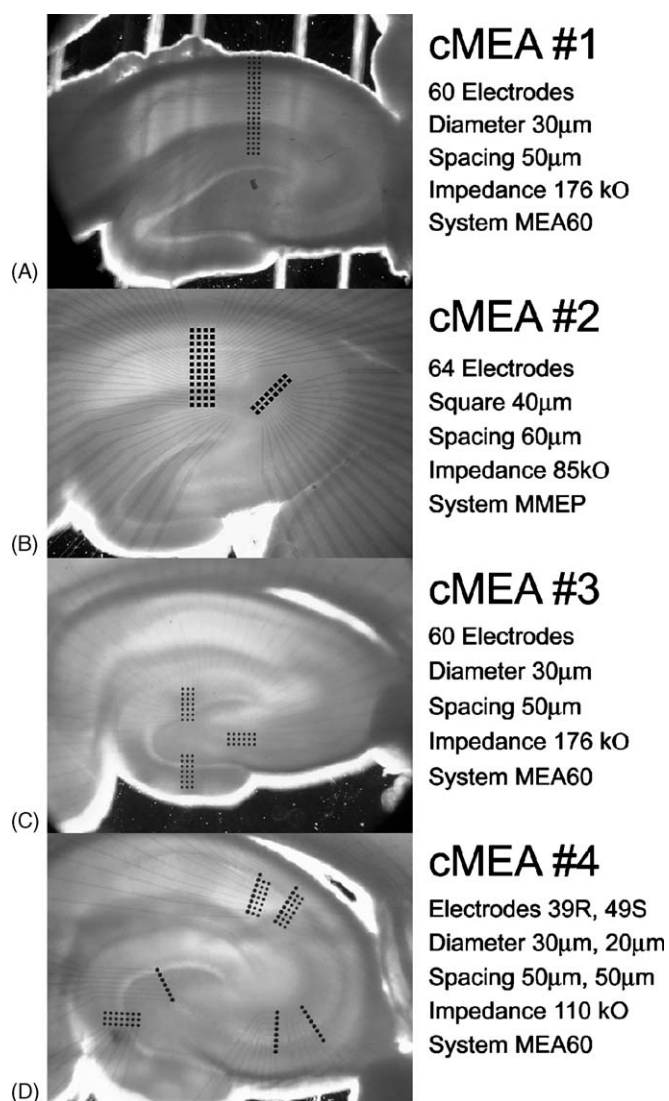


Fig. 1. Conformal probes: (A) cMEA#1 is a 3×20 rectangular array of electrodes. (B) cMEA#2 has a 2×8 sub-array to stimulate Schaffer Collateral (SchC) fibers and a 4×12 sub-array to record output responses from CA1 pyramidal cells. (C) cMEA#3 has two 3×7 sub-arrays to stimulate perforant pathways (PP) and record in dentate gyrus (DG) and one 3×6 sub-array to record CA3 output. (D) cMEA#4 has one stimulation sub-array consisting of seven triplet electrodes aligned to PP, and two other sub-arrays of seven pairs of electrodes for stimulating SchC. Electrodes in pairs or triplets act in unison, as they are connected to each other and lead to one contact pad. cMEA#4 also has four linear sub-arrays of seven or eight electrodes to record from DG, CA3 and CA1.

responses recorded from all four designs. This analysis disentangles field potentials to accurately map sources and sinks of synaptic currents. CSD was combined with sequential stimulations through a column of electrodes to generate a laminar profile of CA1, and to demonstrate independence of spatially distinct inputs. Selective stimulation of afferent fibers was hence optimized with ease even with adjacent pathways. These experiments with acute rat hippocampal slices established that conformal high-density MEAs could be custom-designed for slice preparations to ideally suit experiments requiring selective stimulation of afferent pathways and CSD analysis.

2. Materials and methods

Conformal pMEAs that are hippocampal tissue specific were fabricated. These conformal pMEAs were built to fit into two MEA setups in order to speed up the functional characterization and demonstrate the transferability of the technology.

2.1. Conformal pMEA design and fabrication

Cytoarchitectural measurements were taken from 5 to 10 photomicrographs of hippocampal slices (8–10 weeks old rat). Pyramidal cell layers were extracted and experiment-specific pMEA layouts were superimposed using image analysis software (Illustrator, Adobe, CA, USA). Small groups of electrodes were arranged in sub-arrays perpendicular to their target's cell layer. These electrode arrangements were then laid out using CAD software (L-edit software, Tanner Inc.) where leads and contact arrangements matching one of the electrophysiology recording setups were added for mask design. The cMEAs were then manufactured using standard photolithographic techniques for the selective patterning of the individual layers of the device on a glass substrate. The end product had ITO leads insulated with silicon nitride and SU-8 with the electrode tips coated with gold. The electrodes impedance were measured at 1 kHz (Han et al., 2002).

2.2. Multielectrode setups

Two multielectrode recording systems were utilized: the multi-electrodes-array system (MEA60) and the multi-micro-electrode-plate system (MMEP). Each setup consisted of an electrode array, amplifiers, data acquisition hardware, and its corresponding software. The manufactured pMEAs were designed to interface with one of these two setups. The MMEP is a 64-electrode system (Gross et al., 1993; University of North Texas, <http://www.cnns.org>). Data was amplified 2500× in two stages (Plexon Preamplifiers, <http://www.plexoninc.com>) with cutoff filters at 8 Hz and 3 kHz and was then sampled at 7.35 kHz (Microstar DAQ card, <http://www.mslabs.com>, USA). Separate stimulation boxes (Iso-Flex, AMPI, Israel) allowed programmed (Master-8, AMPI, Israel) bipolar stimulation. The stimulation and recording processes were controlled using a custom written Matlab script.

The MEA60 electrophysiological recording system is a commercially available turnkey system (Multi Channel Systems, Reutlingen, Germany). It consists of amplifiers (1200× gain with a cutoff filters at 0.1–5 kHz), a data acquisition card (10–25 kHz sampling frequency per channel), an eight-channel stimulation box, and collection and analysis software. The software enabled extraction of waveform amplitude and time course display. Further analysis of recorded potentials was conducted in Matlab (The Mathworks, Natick, MA, USA) using the MEAtools toolbox from the University of Freiburg Germany (<http://www.brainworks.unifreiburg.de/projects/meatools/overview.htm>), and custom written scripts for spike amplitude calculations and CSD analysis.

2.3. Acute slice preparation

Young adult male Sprague Dawley rats (1–3 months old or 150–250 g) were anaesthetized with halothane prior to decapitation. Each hippocampus was dissected from the brain and cut transversely along the septo-temporal axis into a single block with entorhinal cortex preservation under cold cutting artificial cerebrospinal fluid (aCSF) consisting of: (in mM) NaCl, 128; KCl, 2.5; NaH₂PO₄, 1.25; NaHCO₃, 26; glucose, 10; MgSO₄, 2; ascorbic acid, 2; CaCl₂, 2, and oxygenated with a mixture of 95% O₂ and 5% CO₂ to maintain physiological pH of 7.2. The tissue blocks were then mounted onto a vibratome (VT1000S, Leica, Germany) with SuperGlue and 400–500 μm thick slices were collected. The slices were incubated at 32 °C in an aCSF for at least an hour before being carefully positioned on an MEA over an inverted microscope (DMIRB, Leica, Germany). The slice position on the MEAs was held constant by a nylon mesh strung across a platinum ring and was documented with a digital camera (Spot RT, Diagnostic Instruments, MI, USA). During the entire experimental duration on the MEAs, slices were submerged and perfused at a constant flow rate of 2 ml/min with aCSF reduced in its MgSO₄ concentration to 1 mM, and was supplemented with 5 μM picrotoxin in the trisynaptic experiments.

2.4. Electrophysiology

Biphasic stimulation of the afferent pathways was performed using either external (bipolar) or internal (monopolar/bipolar) electrodes. External electrodes refer to twisted Nichrome wires that were inserted in the afferent pathway using a micromanipulator. The internal electrodes, on the other hand, refer to single or pairs of microelectrodes in the pMEA that were used for current injection. All stimulation pulses were biphasic with each phase lasting 100 μs. The stimulation protocol consisted of repeated single or paired pulses delivered to the afferent pathway, while the responses were recorded by the pMEA.

2.5. Current source density analysis

CSD was calculated using equation (D3) from Freeman and Nicholson (Freeman and Nicholson, 1975) was applied to the recorded field potentials (FPs):

$$I_m = -\sigma_x(-2\phi_{x-2h} + \phi_{x-h} + 2\phi_x + \phi_{x+h} - 2\phi_{x+2h})/7 \quad (1)$$

where I_m is the current density, ϕ is the FP at location x , σ is an estimate of biological tissue conductivity along the analyzed dimension, and h is the spatial sampling interval along that dimension. One-dimensional CSD was preferred to two-dimensional CSD because the five points CSD equation (D3) yielded smoother results. This equation could not be applied along the two planar dimensions because the cMEAs do not have 5 × 5 electrode grids. CSD was calculated using raw and filtered data (low pass spatially filtered field potentials (Shimono et al., 2002)). There was no difference between the two sets because the D3 equation already includes a low pass smoothing spatial filter (Lanczos, 1956).

FP and CSD topographical activity maps were generated in Matlab by assigning a color scheme to the measurement range and applying piecewise cubic Hermite interpolation between vertical electrodes data values. The 10 kHz sampling rate eliminated the need for interpolation along the time domain. Data overlays on slice images were accomplished in Photoshop (Adobe, San Jose, CA, USA).

3. Results

3.1. Fabrication results

Four configurations of high-density cMEA were designed and manufactured to conform to hippocampal slice cytoarchitecture in order to stimulate and record electrical activity in specific areas. The impedance measurements were measured at 1 kHz in an aCSF analyte in order to mimic experimental conditions. The cMEA#1 is a 3×20 design (Fig. 1A). Each electrode has $28 \mu\text{m}$ diameter with $50 \mu\text{m}$ inter-electrode distance ($176 \text{ k}\Omega$). The 3×20 rectangular was designed for electrophysiological investigations of the pyramidal and granular cells of the hippocampus. The cMEA#2 is a $2 \times 8 + 4 \times 12$ design (Fig. 1B). The electrodes had a square size of $36 \mu\text{m} \times 36 \mu\text{m}$ ($85 \text{ k}\Omega$) and an inter-electrode distance of $60 \mu\text{m}$. The 2×8 and the 4×12 sub-array were intended for the Schaffer Collateral pathway stimulation optimization and for the recoding of the corresponding CA1 response respectively. The cMEA#3 is the $3 \times 7 + 3 \times 7 + 3 \times 6$ design (Fig. 1C). Each electrode had a $28 \mu\text{m}$ diameter with $50 \mu\text{m}$ inter-electrode distance ($176 \text{ k}\Omega$). This pMEA was designed in such a manner that $3 \times 7 + 3 \times 7$ sub-arrays would be optimal for the medial and lateral PP stimulation and for the recording of the DG response. The 3×6 sub-array was placed in the CA3 region in order to record CA3 disynaptic response resulting from the PP stimulation (PP \rightarrow DG \rightarrow CA3). The cMEA#4 (Fig. 1D) is complex array that was designed to record the trisynaptic activity along the hippocampal circuitry and to perform a proof of concept of cortical prosthetics by replacing the CA3 functionality in vitro (Berger et al., 2001, 2005b, 2005a). The cMEA#4 includes two different circular pad sizes: (1) $28 \mu\text{m}$ diameter pads with a $50 \mu\text{m}$ inter-electrode spacing grouped in series to form sets of stimulating pads in dentate gyrus (DG) (three at a time) and CA1 (two at a time); (2) $36 \mu\text{m}$ diameter pads also with a $50 \mu\text{m}$ center-to-center spacing ($110 \text{ k}\Omega$) for recording the trisynaptic activity in DG, CA3, and CA1. The stimulating electrodes were connected in pairs or triplets to allow larger stimulation currents because it is believed that increased perimeter to area ratio minimizes the effect of the inhomogeneous charge distribution and enhances diffusive flux to the electrode edge (Rubinstein et al., 1987; Stulik et al., 2000). A sub-array of seven triplets was positioned to stimulate PP, and two sub-arrays of seven pairs targeted SchC. Linear sub-arrays of seven to eight electrodes conformed to record outputs from primary excitatory cells in DG, CA3 and CA1.

Due to the large size of the pMEA glass support ($49 \text{ mm} \times 49 \text{ mm} \times 1 \text{ mm}$), up to six arrays can be manufactured at one time in academic fabrication facilities over the

period of 1 week. However, once all fabrication parameters were defined, pMEAs could be reproducibly manufactured and over 30 pMEAs have been produced. It is worth noting that the use of SiN_x films as etch masks and etch-stops increased production yield due to their superior adhesion to the substrates and their resistance to etchants, in contrast to well-processed photoresist mask layers, which suffered from undercuts. This additional use of SiN_x as wet etching mask did not increase fabrication time since multiple substrates can be deposited simultaneously with each manufacturing cycle. These pMEAs were durable, and some have been used to record useful signals in over 30 experiments, each consisting of hundreds of stimulations. Electrode impedance and stimulation capacity varied depending on tip design. Electrochemical characterization of these electrodes by impedance measurements, cyclic voltammetry and current injection limits determination has been previously described (Han et al., 2002).

3.2. Electrophysiological recordings from the arrays using external stimulation

The ability of cMEAs to record extracellular FPs was assessed by stimulating acute slices with external electrodes made of twisted nichrome wire. Using cMEA#2, monosynaptic input/output (IO) curves were recorded in CA1 in response to SchC stimulation with electrical pulses of increasing intensities that ranged from 200 to $1000 \mu\text{A}$ (Fig. 2). The output was a measure of the corresponding FP amplitude recorded in the pyramidal cell layer, and calculated as the difference between the recorded waveform's minimum and maximum. The signal-to-noise ratio exceeded 10:1, where noise was calculated as root-mean-square (RMS) of the potential before stimulus. Well-defined population spikes overriding excitatory postsynaptic potentials (EPSP) were observed at high stimulation intensities. Electrodes on the basal side of the pyramidal layer recorded the largest population spikes, whose maximum amplitudes were in the range $150\text{--}250 \mu\text{V}$. Fig. 2B shows an overlay of sample responses at different intensities, and Fig. 2C plots the average of five IO curves at equivalent basal recording sites from five different slices. Response amplitude increased linearly until it saturated at higher stimulation intensities.

Monosynaptic and disynaptic responses were similarly recorded from DG and CA3 respectively by stimulating PP with external electrodes (Fig. 3). The stimulation protocol consisted of paired pulses with 30 ms inter-stimulus intervals (ISI), which facilitated disynaptic responses. Monosynaptic population spikes were recorded in the dorsal and ventral blades of DG (Fig. 3A and B). Disynaptic responses in CA3 had spike latencies in the range 6–9 ms in relation to the DG monosynaptic population spike (Fig. 3C).

The cMEA#4 was designed to record the monosynaptic response of the DG, disynaptic response in the CA3 area and trisynaptic response in the CA1 when the PP is stimulated. The recordings were used to build a nonlinear dynamic model of the CA3 (Berger et al., 2005a; Gholmieh et al., 2002, 2003) by stimulating the PP intermittently with Poisson-distributed electrical pulses (random intervals with an average frequency

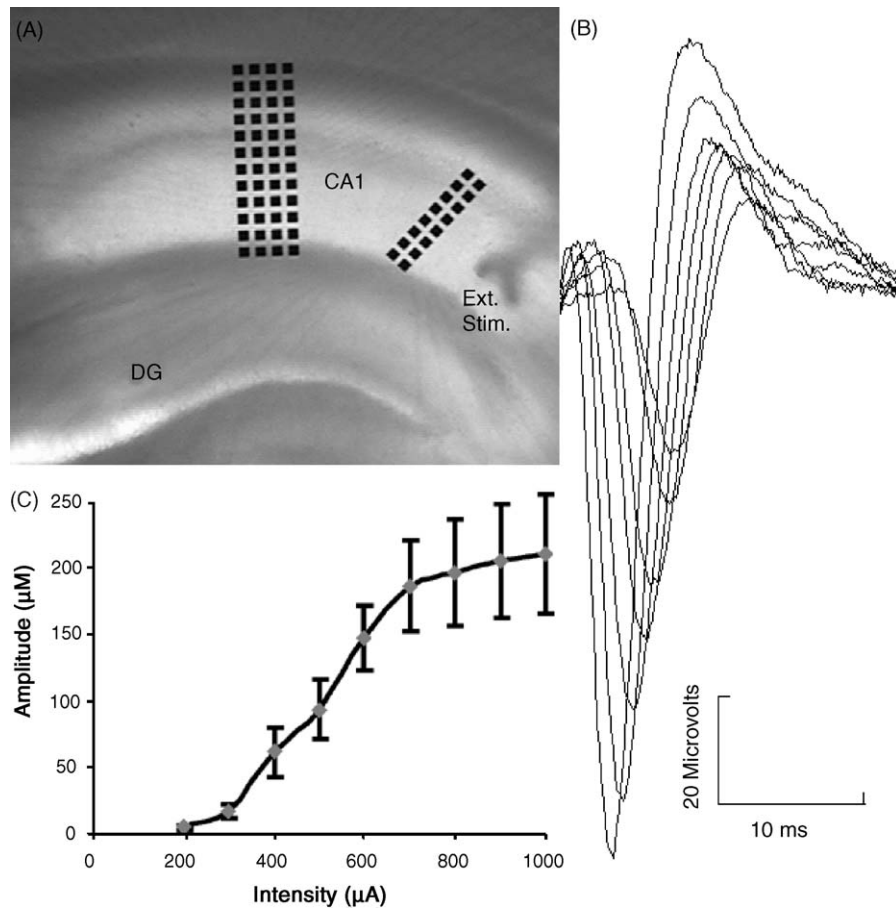


Fig. 2. (A) Photomicrograph of a hippocampal slice positioned over cMEA#2. The tip of a twisted nichrome external stimulating electrode is visible inside the slice to the right of the stimulation sub-array. (B) Overlay of population spike responses at increasing stimulation intensities. (C) Graph of average and standard deviation of the mean of five IO curves at equivalent basal recording sites from five different slices.

of 2 Hz). The recordings were facilitated by using 5 μM picrotoxin that partially paralyzed the GABAergic inhibition in the neuronal circuitry. The cMEA#4's recording electrode positions enabled recording population spikes in the DG and CA3 and dendritic EPSPs in CA1 simultaneously without perturbing the slice or damaging it by repeated electrode insertions to find optimal recording sites (Fig. 4 A and B). Population spikes and EPSPs had delays commensurate with synaptic separation (Fig. 4C). The model required multiple data collections using several slices and over extended period of time. In each session, an IO curve was obtained and then greater than 1200 pulses were used to stimulate the PP for more than one hour. The elicited trisynaptic responses were stable and showed different latencies (CA1 > CA3 > DG). Fig. 4D shows a trisynaptic response at the end of the stimulation session that was similar to the trisynaptic response at the beginning of the recording session (Fig. 4C).

3.3. Stimulation pathway selection

3.3.1. SchC-CA1 stimulation and recording optimization

The primary advantage of cMEA#2's conformal design was in the ease and convenience of optimizing stimulation and

recording locations. Hippocampal slices were positioned such that the 2×8 sub-array crossed the SchC pathway, and the 4×12 sub-array was aligned to the axo-dendritic axis of CA1 pyramidal cells (Fig. 5 A). The eight electrodes in the left column of the 2×8 sub-array were used for bipolar stimulation in seven adjacent pairs: S1-2, S2-3, . . . , S7-8 (Fig. 5A, inset). Paired-pulses of 30 ms ISI and 70–100 μA were delivered sequentially through each pair to identify the location that yielded the largest amplitude population spike. The left most column of the 4×12 sub-array was used for recording (R column, Fig. 5A inset). The largest response for this slice was obtained through stimulation from pair S5–S6, as shown in the stimulation optimization graph which plots the spike amplitude versus the different stimulation pairs (Fig. 5B). In each of six slices, one optimal stimulation pair was observed. That stimulation pair was then used to generate an IO curve, by incrementally increasing the stimulation intensity over a 10–250 μA range. The stimulation intensity was then set to yield half maximal response, and five sets of paired pulses were delivered again through each of the seven electrode pairs and then averaged. The laminar profile recorded in the R column for the slice shown in Fig. 5A indicated the largest pyramidal population spike at R11 and the largest dendritic components at R3 and R4 (Fig. 5C).

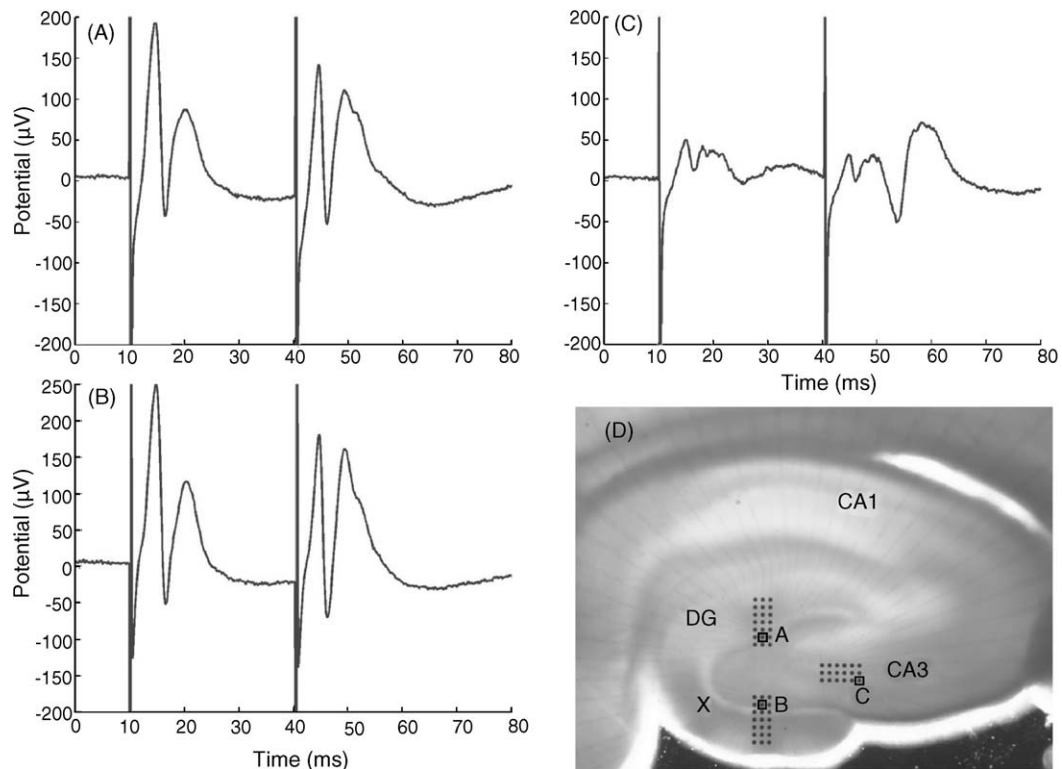


Fig. 3. Mono- and di-synaptic responses evoked by paired pulse stimulation from wire electrodes and recorded with cMEA#3. (A) Monosynaptic population spikes recorded from the DG's dorsal (A) and ventral (B) blades. (C) Di-synaptic population spikes recorded from CA3 were more prominent in response to the second pulse. (D) Photomicrograph of the corresponding hippocampal slice positioned over cMEA#3. The stimulation electrode is discernible as a dark area in the corner of DG marked with an X.

3.3.2. Selective stimulation of medial and lateral PP

The cMEA#3 had three sub-arrays designed to study PP-DG-CA3 synapses with an emphasis on differentiating between lateral and medial PP fibers. These sub-arrays span outer and inner blades of DG and CA4/CA3 in hippocampal dorsal slices (Fig. 6 A). In order to demonstrate the ability to discriminate between these two pathways using a high-density conformal cMEA, the lateral and medial PP were stimulated using pairs of electrodes in DG outer blade in five different slices. Stimulation in lateral PP produced paired pulse facilitation with a 13.58% (S.E.M. \pm 4.1%) increase in amplitude of the second dentritic fEPSP (Fig. 6B). Medial PP stimulation resulted in paired pulse depression with a 13.86% (S.E.M. \pm 1.6%) decrease in the amplitude of the second fEPSP (Fig. 6C). The selected electrode pairs clearly stimulated the two PP pathways based on their anatomical location and responses. This fine spatial control over stimulation is much more difficult to obtain using more sparsely arranged pMEAs and nearly impossible to achieve in a single slice with external wire electrodes.

3.4. Current source density analysis of CA1 pyramidal cells

In order to assess the applicability of high-density pMEAs for CSD analysis, hippocampal slices were oriented on cMEA#1 such that CA1's pyramidal axo-dendritic axis was parallel to the longest side of the rectangular array (Fig. 7 A). Monopolar biphasic stimulations were then delivered through one of the

electrodes in a peripheral column, and evoked responses were recorded from the remaining 59 electrodes. The left panel in Fig. 7B shows FP activity recorded at the middle column of electrodes in response to a single stimulation in *stratum radiatum* (marked by a red dot). Positive FPs were observed in *stratum oriens* and negative potentials in *stratum radiatum* and *moleculare* with a 3–5 ms delay. Population spikes were then seen as a sharp deflection in the waveform with a 5 ms delay. These currents gradually switched polarity as cells repolarized themselves, and hyperpolarized 20 ms after stimulation. Simultaneous recordings along the length of pyramidal cells constituted a FP laminar profile of CA1 responses. By interpolating between adjacent recordings, a topographical map was generated in which voltages were assigned colors (Fig. 7B). In these color maps, yellow/red marked the spread of positive EPSPs, while blue areas delineated negative EPSPs, or the spread of population spikes through positive EPSPs. The spatial spread of population spikes was markedly narrower in CSD topographical maps (Fig. 7B). CSD also more finely localized reversal regions of EPSPs and population spikes (zones where their polarity inverts) to *stratum pyramidale*. Additionally, CSD analysis unmasked a current source in *stratum radiatum* that was not discernible in FPs.

After illustrating the classical advantage of CSD over FP, the effect of different electrode densities on CSD resolution was investigated. FP recordings from a 20 electrode column were separated into groups of 10 odd and 10 even electrodes, and CSDs from these subgroups were compared to CSDs obtained

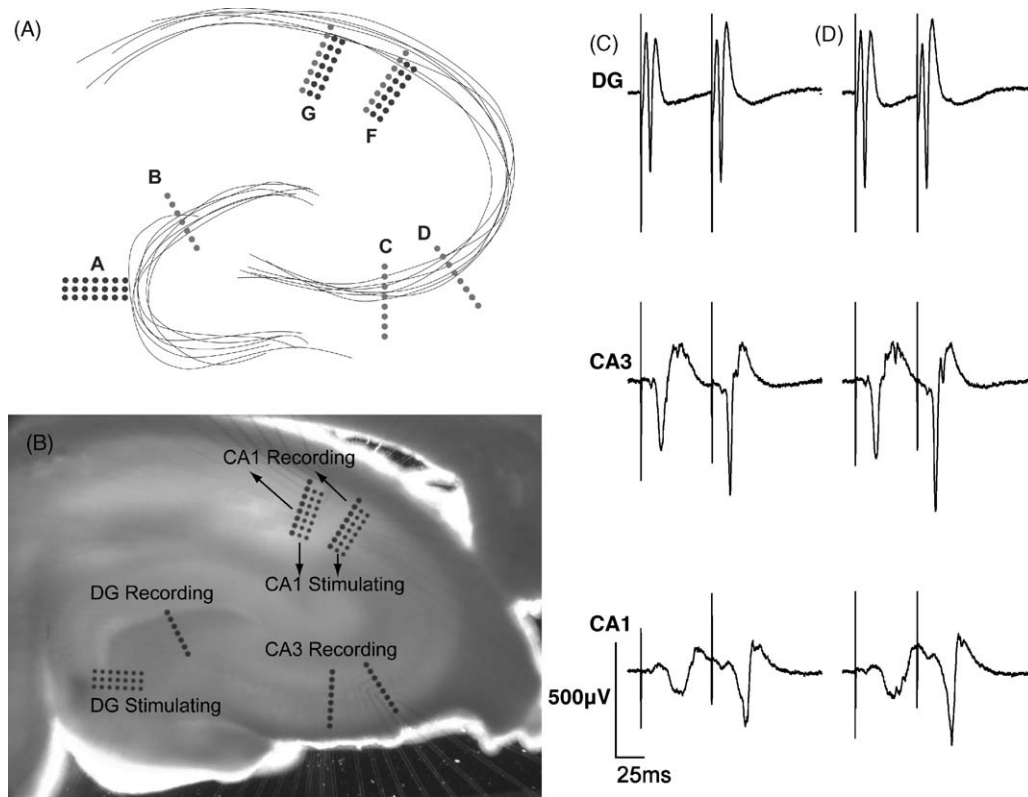


Fig. 4. Monitoring trisynaptic activity in hippocampal slices with cMEA#4. (A) The design of the conformal multi-electrode array included two different circular pad sizes: ((A) 3×7 and (F and G) 2×7) $28 \mu\text{m}$ diameter pads with a $50 \mu\text{m}$ center-to-center spacing grouped in series to form sets of stimulating pads in DG and CA1, and ((B) 1×7 and (C, D, F, and G) 1×8) $36 \mu\text{m}$ diameter pads also with a $50 \mu\text{m}$ center-to-center spacing for recording. The sets are aligned according to rat hippocampal cytoarchitecture covering key input/output regions of DG, CA3, and CA1, thereby allowing complete diagnostic assessment of the nonlinear dynamics of the trisynaptic circuit. (B) Photomicrograph of a slice on the cMEA. (C) Trisynaptic recording from the DG, CA3 and CA1 areas. PP stimulation yielded large populations pikes in DG and CA3 and an EPSP in CA1, all with the appropriate multi-synaptic time delays. (D) Paired pulse responses from the same slice recorded after (C) and following 1200 stimulations with random intervals. Scale bars 20 ms and $500 \mu\text{V}$.

from the entire 20 electrode column. Fig. 8 shows FPs and CSDs obtained from a single stimulation at an electrode in *stratum radiatum* (same as in Fig. 7). Topographical maps indicated that for a same stimulation, there was minor difference between data collected on odd and even subgroups, mostly consisting of slight signal size variations. The most significant observation was the effect of electrode separation on CSDs, whereby CSD from even and odd subgroups, whose electrodes were separated by $100 \mu\text{m}$, did not narrow sinks and sources as did CSD from the entire array with $50 \mu\text{m}$ inter-electrode spacing.

CSD analyses of multiple laminar profiles of CA1 were generated by sequentially stimulating electrodes in a column along the entire length of the pyramidal cells. Fig. 9 shows CSDs of laminar profiles recorded from the middle column of the array depicted in Fig. 7, with stimulus sites denoted by red dots. The stimulation spanned the entire dendritic range of CA1 and into DG. Starting with stimulation under alvear fibers, where the slice has less thickness due to slicing along the hippocampal curvature, no response was generated (profiles 1–3). As the stimulation site moved closer to the cell body layer, a current sink was observed in the *stratum oriens* with a corresponding source in *stratum pyramidale* (profiles 4–7). Exciting the cell body layer directly produced smaller sinks and sources (profile 8), which inverted in polarity for stimuli at *stratum radiatum* (pro-

file 9). As the stimulating site moved more distally along the apical dendritic tree, sinks and sources first grew to their largest values (profiles 10 and 11) and then gradually decreased (profiles 12–14) until the stimulation site reached *stratum lanucom-moleculare* (profiles 15–17), yielding no evoked responses. Stimulating close to the fissure did not produce responses in either CA1 or the DG (profile 18). Finally, large current sinks in the last two profiles (profiles 19 and 20) were responses of granule cell dendrites to stimulation in *stratum moleculare* of DG.

4. Discussion

Few tissue and experiment specific cMEA configurations have been produced in order to circumvent limitations resulting from fixed numbers of channels currently available in pMEA recording systems: (1) a hexameric layout with smaller and closer electrodes in its center for retinal recordings (multi channel systems) and (2) elliptic (Thiebaud et al., 1997) or circular (Dupont et al., 1999) electrode layouts designed for hippocampal slices with a single or double layer of electrodes matching roughly the cytoarchitecture of hippocampal pyramidal cells. These latter arrays, however, are hard to align with the tissue due to differences in animal brain size and slicing. Additionally,

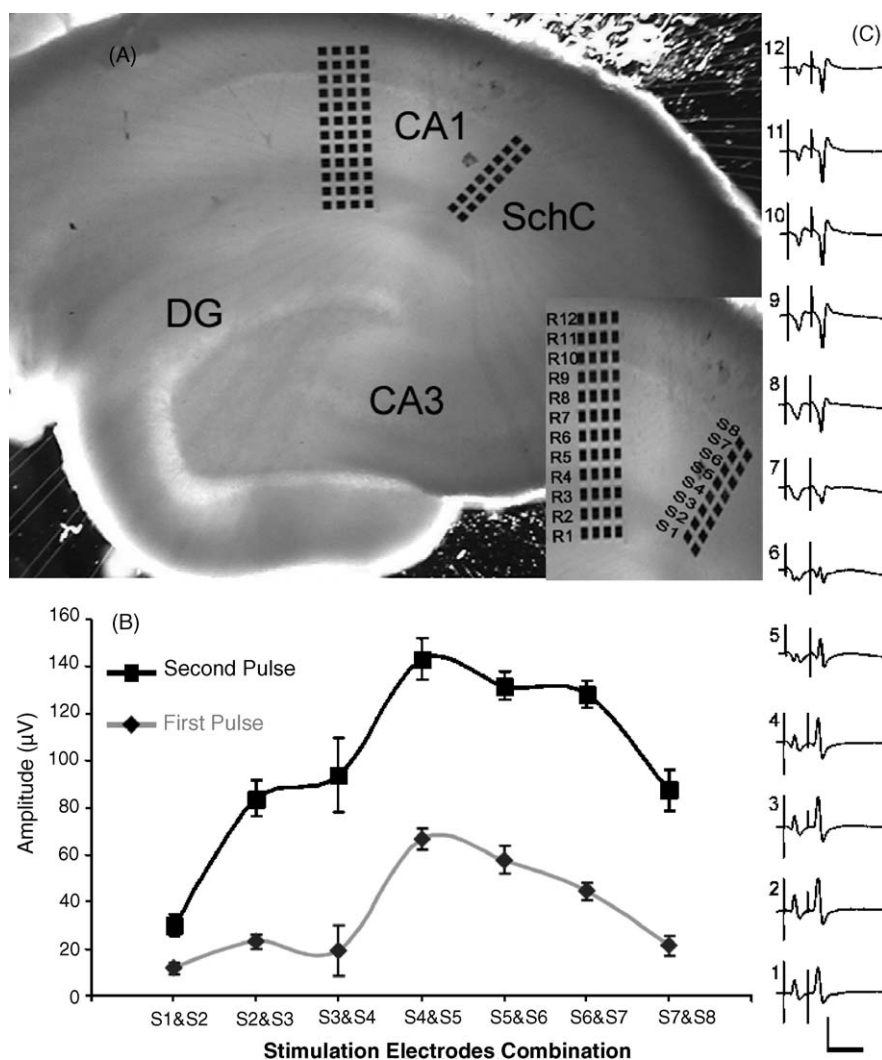


Fig. 5. Optimization of stimulation and recording at SchC-CA1 synapse. (A) Hippocampal slice on cMEA#2. Inset: blow-up of recording (R column is left most) and stimulation sites (S column is left most in its sub-array). (B) Graph of average and standard error of the largest population spike amplitudes recorded from a slice and plotted against stimulation pair. Responses amplitude to paired pulse stimulation are shown in gray for the first pulse and black for the second pulse. (C) Laminar profile of FPs recorded at leftmost column R electrodes in response to paired pulse stimulation at electrodes S4–S5. Scale bar 50 ms and 100 μ V.

none of these MEAs are optimized for current source density (CSD) analysis, which requires 50 μ m inter-electrode distance (Wheeler and Novak, 1986). This paper introduces four high-density pMEAs that are well suited for specific electrophysiological applications and CSD analysis.

The key parameters of each fabrication technique were empirically derived, providing for repeatable, time-efficient and high-yield reproduction capacity. ITO was chosen as a substrate for connecting leads because it is transparent and allows visualizing of the tissue on top of cMEAs. The dual SiNx/SU-8 insulating layer allowed for a decrease in shunt capacitance and provided durability so that a consistent SNR was obtained after repeated acute slice tests. Several experiments were performed to demonstrate the physical characteristics, and the functionality of the pMEAs, as well as to illustrate the advantages of conformal designs. These cMEA were used repeatedly in over 20 experiments involving acute slices with stable signal to noise ratio. The stability of the recording was shown in the experiment that used the cMEA#4 where trisynaptic field potentials data was stable

over the period of recording/data collection and post 1200 stimuli. It is worth to note, however, that the 50 μ m dead cell layer at the slice surface prevents the recording of single unit activity which is usually observed with tissue-penetrating extracellular electrodes and dissociated cell cultures.

The electrophysiological experiments performed using external stimulation established the functionality of the high-density arrays by recording physiologically sound data. The observed waveforms exhibited a signal-to-noise ratio greater than 10:1 (Figs. 2B, 4A and 5A–C) and were similar in properties to the ones recorded with single sharp-tip glass electrodes (Leung and Fu, 1994). The graded monosynaptic responses that were observed in CA1 region followed the typical sigmoidal shape of an IO curve obtained in CA1 (Fig. 4B). The negative going population spike overriding the positive EPSP was best observed slightly basal to the pyramidal layer in the region corresponding to the axonal hillock region. This result is in agreement with previous studies (Brankachk and Buzhaki, 1987; Richardson et al., 1987) that showed the “initial site for generation of a spike

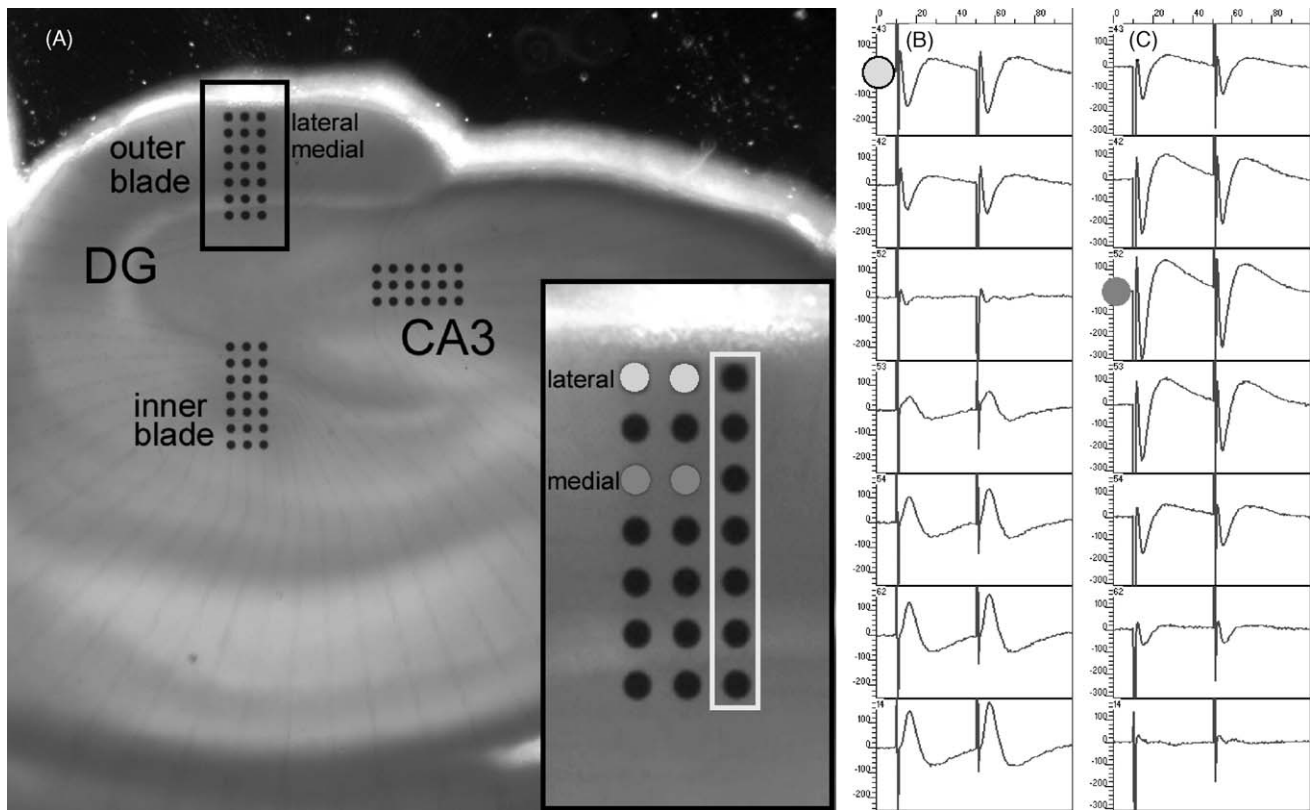


Fig. 6. Paired-pulse facilitation and depression in DG. (A) Photomicrograph of DG on cMEA#3 with inset showing close-up of stimulation sub-array under outer blade. Electrodes in light and dark gray correspond to lateral and medial perforant path stimulation sites respectively. (B) Paired-pulse facilitation at electrodes in column demarked by gray rectangle in (A) to bipolar stimulation in lateral PP. (C) Paired-pulse depression in response to medial PP stimulation. The interstimulus interval was 50 ms. Y-axis range: -300 to $200 \mu\text{V}$. X-axis span: 100 ms.

along the dendrosomatic axis of the pyramidal cell following antidromic or orthodromic stimulation is in the region of the cell body layer (soma or axon hillock)". Perforant path stimulation using the cMEA#3 lead to monosynaptic and disynaptic responses in the Dentate and CA3 regions, respectively. The disynaptic response in the CA3 region exhibited a delay in the range 7–10 ms and showed paired pulse facilitation consistent with mossy fibers and CA3 pyramidal cells known characteristics (Hussain and Carpenter, 2003).

Stimulation through the cMEA proper electrodes enabled fine tuning of the stimulation sites. The cMEA#2 was designed for finer control over the input-output properties of CA3–CA1 regions of the hippocampal slice. The 2×8 sub-array was designed to stimulate SchC and the 4×12 sub-array to record from the corresponding CA1 somatic and dentritic response. The stimulation and recording were optimized by selecting the electrodes that yielded the maximal response. Across different slices, the single peak observed in the stimulus optimization graph suggested that a narrow strip of axons was the dominant afferent input. Such a fiber bundle can be easily localized and targeted using this conformal pMEA. Moreover, the relatively large distance between the stimulation and the recording sub-arrays enabled higher stimulation intensities ($>150 \mu\text{A}$) without distorting the evoked responses with the stimulus artifact.

A further exploration of finer control over the stimulation paradigm was illustrated using the PP-Dentate-CA3 array

(cMEA#3) where two adjacent afferent pathways were selectively stimulated and differentiated using high-density arrays designed to match the anatomical area. PP is the main input to the DG, and it is divided into two anatomically distinct subregions: lateral and medial. The lateral PP originates in the lateral entorhinal cortex and synapses on the outer third of the molecular layer of the dentate gyrus while the medial PP projects from the medial entorhinal cortex to the middle third of the molecular layer (Steward, 1976). Though the two pathways are functionally distinct (Dahl et al., 1990; McNaughton and Miller, 1984), studies of DG electrophysiology often do not specify which subdivision is being stimulated. Experimentally, the subdivisions are distinguished by their response to paired pulse stimulation: the lateral PP shows a facilitated second response, while the medial displays paired pulse depression. This was illustrated in Fig. 6 where the lateral PP exhibited paired-pulse facilitation mostly in the lateral molecular layer, while the medial PP produced paired-pulse depression in the medial molecular layer. The $50 \mu\text{m}$ interelectrode spacing enabled the selection of accurate stimulation sites in each pathway without disturbing the tissue by repeated wire electrode insertions. This experiment demonstrated the ease with which pathway subdivisions can be selectively stimulated and their responses distinguished using high-density pMEAs.

The advantage of simultaneous multi-site recording was illustrated using the cMEA4. This MEA was designed to record

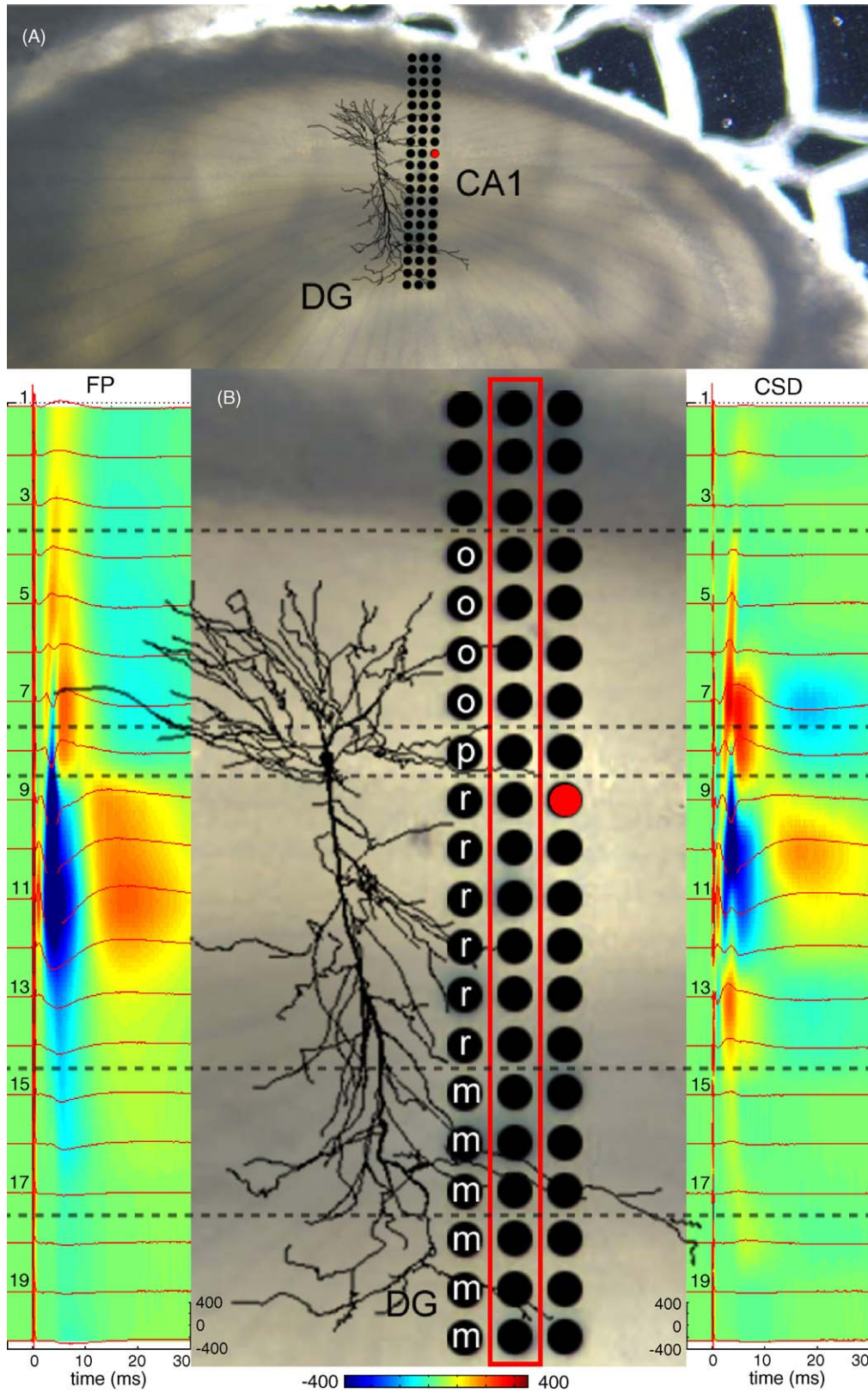


Fig. 7. FP and CSD of pyramidal cell activity. (A) Photomicrograph of a hippocampal slice on cMEA#1 with a pyramidal cell drawing from the Neuron Morphology Database (<http://neuron.duke.edu>) to illustrate spatial extent of cells and strata relative the electrodes. (B) Expansion of cMEA's span of CA1 and laminar profile recorded in response to 50 μA monopolar stimulation at the electrode marked in red. The red traces show recorded FP or calculated CSD from the middle electrode column (red box), with numbers corresponding to electrode position starting from the top. Topographical maps converted voltage to a color scale ($-400 \mu\text{V}$ (blue) to $400 \mu\text{V}$ (red)) and interpolated values between the electrodes. Strata are marked with a dashed line and labeled in white along the electrodes [o: oriens; p: pyramidale; r: radiatum; m: moleculare (CA1 and DG)] and trace drawing of a pyramidal cell. 200 μA stimulation triggered 5 ms after recording onset. X-axis span: 35 ms.

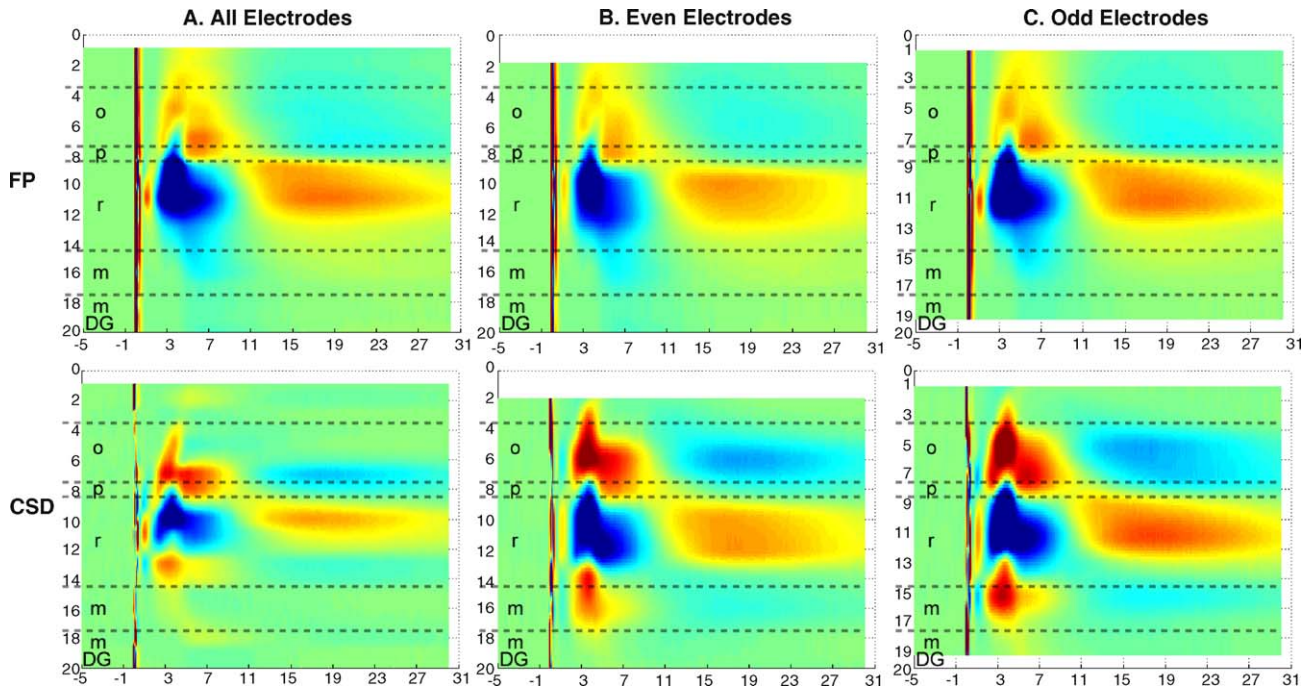


Fig. 8. Electrode separation affected spatial resolution of CSD but not FP's. FP and CSD laminar profiles of the response shown in Fig. 7 constructed from: (A) all 20 electrodes in a column ($50\ \mu\text{m}$ interelectrode separation) and from subsets of (B) 10 odd and (C) 10 even electrodes ($100\ \mu\text{m}$ separation). The slice, stimulation site and intensity, and color scale are the same as in Fig. 7, and strata are marked with a dashed line.

trisynaptic data (Yeckel and Berger, 1990) from three subregions of the hippocampus in response to the PP stimulation. The recordings were used to build a nonlinear dynamic model of the CA3 (Berger et al., 2005a; Gholmieh et al., 2002, 2003) by stimulating the PP with Poisson-distributed electrical pulses (random intervals). Recording from the three subregions using traditional glass electrodes involved the cumbersome and time-consuming positioning of three glass electrodes and the stimulating electrode (Pare and Llinas, 1994). The cMEA#4 expedited data collection by placing the electrodes at specific sites for a specific experimental objective and provided a test bed for a cortical prosthesis (Berger et al., 2005a).

CSD analysis is a mathematical technique that converts field potentials (FPs) measured at different locations into a spatial distribution of electrical currents, by using information from adjacent recording sites (Freeman and Nicholson, 1975; Nicholson and Freeman, 1975; Nicholson and Llinas, 1975). Neuronal cells, which are embedded in a conductive medium, generate transmembrane sinks (inward currents) and sources (outward currents) along the axons, soma, and dendrites. These sinks and sources form additive FPs, and therefore the true current distribution and amplitude do not necessarily parallel those of the recorded FPs. The CSD thus compensates for the diffuse resolution of the FP and localizes the true sinks and sources of the electrophysiological activity.

Laminar profiles of FPs and CSDs were generated in response to stimulation of SchC using Design#1 (Fig. 7B). The $50\ \mu\text{m}$ inter-electrode distance made the pMEAs fit for CSD analysis. In fact, previous simulation results indicated that this is the minimum acceptable spatial resolution for CSD analysis in the

Hippocampus in vitro (Wheeler and Novak, 1986). As expected, the CSD analysis narrowed the current sink and uncovered an additional current source in *stratum radiatum*, thus providing a better spatial map of the synaptic current responses along the dendrites than the raw FPs (Nicholson and Freeman, 1975). The theoretical limit on the inter-electrode distance was further explored by comparing the effects of lower spatial resolution on the calculated CSD.

The CSD analyzed from data obtained with 20 electrodes showed narrower sinks and sources when compared to those calculated from data from two 10 electrodes subgroups (Fig. 8). The odd group color map appeared more intense than the even one, probably due to different values in the FPs of those subsets. This difference may be due to variations in electrical activity along the extent of the pyramidal cells. This observation points to the importance of electrode placement in FP recordings, and alludes to the variability that can be expected from single electrode recordings. The distribution of synaptic responses was thus more accurately delimited by more precise mapping of the current sinks and sources obtained from arrays with $50\ \mu\text{m}$ inter-electrode distance.

CSD of multiple laminar profiles of the pyramidal cells in CA1 were obtained through sequential stimulation of one peripheral column of the cMEA#1. The profiles obtained mapped the distribution of the inputs onto CA1 pyramidal cells. Basal side stimulation generated a sink at *stratum oriens* and a source around the pyramidal layer, which was of the opposite polarity to when the stimulus was in *stratum radiatum*. Exciting the cell body layer directly evoked a smaller response, which is in accordance with its lower number of synaptic inputs. These

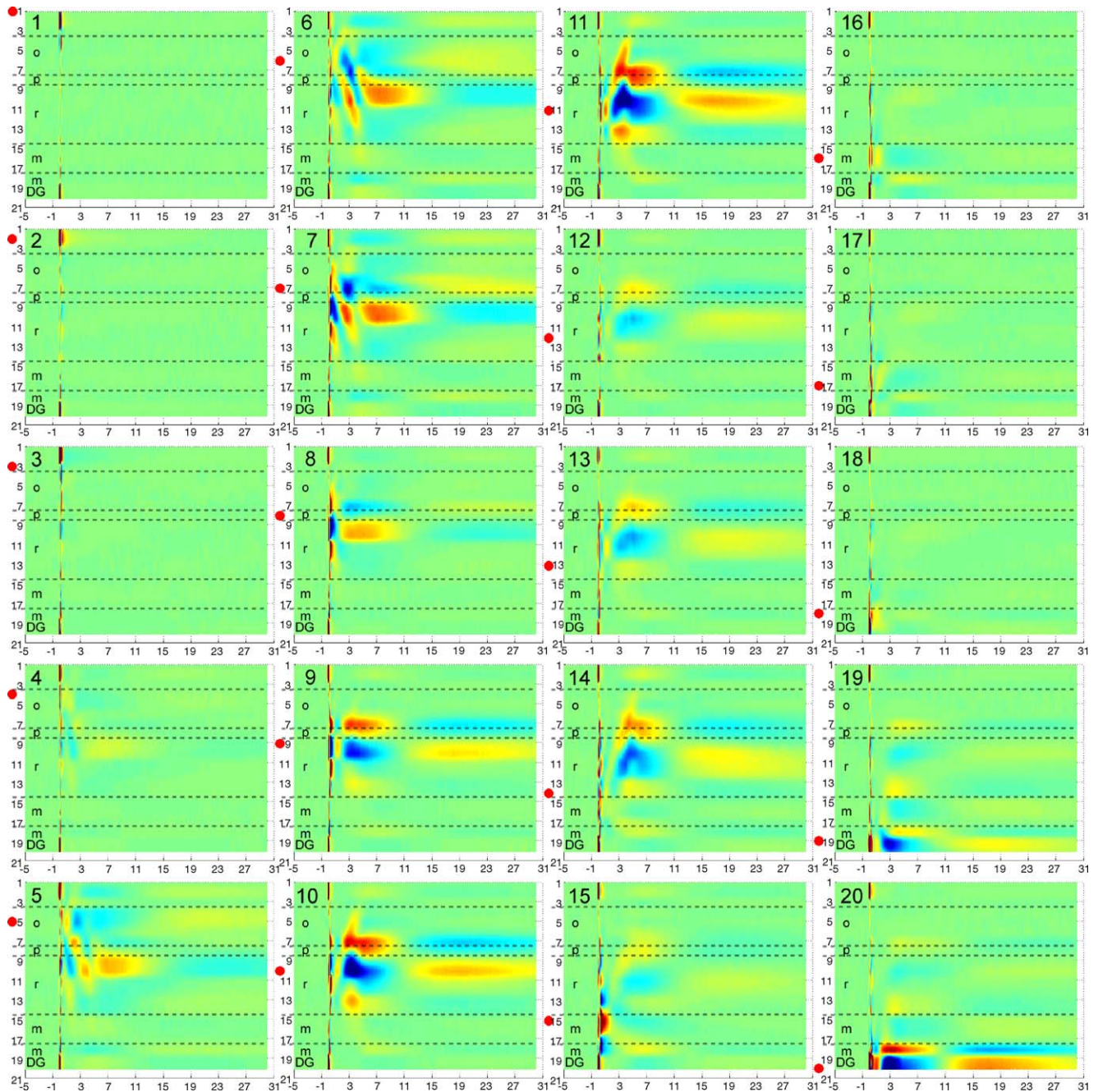


Fig. 9. Laminar response profile of CA1. CSD topographical color maps of laminar profiles of the slice in Fig. 7 in response to sequential stimulations along a peripheral column. The red dot marks the stimulation electrode's relative position for each panel, with stimulation starting basal to the pyramidal layer in stratum oriens and proceeding into DG's stratum moleculare. The slice, stimulation intensity, and color scale are the same as in Fig. 7, and strata are marked with a dashed line.

results are consistent with the neuroanatomy of the CA1 region (Andersen, 1975), where SchC and commissural fibers project to both *strata radiatum* and *oriens* forming two excitable pathways (Buzsaki and Eidelberg, 1982; Richardson et al., 1987).

In summary, rapid transition of cell types in the brain mandates high spatial resolution while the asymmetrical organization of the brain coupled with the limited number of recording channels requires conformal design. We have presented in this article *in vitro* electrophysiological results from acute hippocampal slices that illustrate the advantages of the conformality and

high-density aspects of the successfully fabricated pMEAs. The conformality enabled precise and convenient noninvasive selection of stimulation and recording sites in a specific region of the slice, while the high-density aspect provided sufficient spatial resolution for CSD analysis. The demonstrated capabilities of the conformal pMEA can be used for many different applications such as extracellular acute slice recordings (Oka et al., 1999), long-term monitoring for tissue based neurotoxins biosensors in which electrophysiological activity of a hippocampal slice culture is used to detect and identify toxic and hazardous chem-

ical (Gholmieh et al., 2001; Shimono et al., 2002), or for the development of cortical implants (Berger et al., 2001).

References

- Andersen P. Organization of hippocampal neurons and their interconnections. In: Isaacson RL, Pribram KH, editors. *The hippocampus*, vol. 1. New York: Plenum Press; 1975. p. 155–75.
- Berger TW, Baudry M, Brinton RD, Liaw JS, Marmarelis VZ, Park AY, et al. Brain-implantable biomimetic electronics as the next era in neural prosthetics. *Proc IEEE* 2001;89(7):993–1012.
- Berger TW, Ahuja A, Courellis SH, Deadwyler SA, Erinjippurath G, Gerhardt GA, et al. Hippocampal-cortical neural prostheses to restore lost cognitive function. *IEEE Trans Biomed Eng* 2005a;24(5):30–44.
- Berger TW, Gholmieh G, Hsaio MC, Song D, Granacki JJ, Wills J, et al. Implantable biomimetic electronics as neural prostheses for lost cognitive function. In: *Proceedings of the sixth Asian-Pacific conference on medical and biological engineering (APCMBE2005)*; 2005b.
- Boppart SA, Wheeler BC, Wallace CS. A flexible perforated microelectrode array for extended neural recordings. *IEEE Trans Biomed Eng* 1992;39(1):37–42.
- Borkholder DA, Bao J, Maluf NI, Perl ER, Kovacs GT. Microelectrode arrays for stimulation of neural slice preparations. *J Neurosci Meth* 1997;77(1):61–6.
- Brankachk I, Buzhaki D. Spatial distribution of hippocampal responses to dental pulp stimulation and acoustic clicks. *Neurofiziologija* 1987;19(1):36–46.
- Buzsaki G, Eidelberg E. Convergence of associational and commissural pathways on CA1 pyramidal cells of the rat hippocampus. *Brain Res* 1982;237(2):283–95.
- Dahl D, Burgard EC, Sarvey JM. NMDA receptor antagonists reduce medial, but not lateral, perforant path-evoked EPSPs in dentate gyrus of rat hippocampal slice. *Exp Brain Res* 1990;83(1):172–7.
- Droge MH, Gross GW, Hightower MH, Czisny LE. Multielectrode analysis of coordinated, multisite, rhythmic bursting in cultured CNS monolayer networks. *J Neurosci* 1986;6(6):1583–92.
- Duport S, Millerin C, Muller D, Correges P. A metallic multisite recording system designed for continuous long-term monitoring of electrophysiological activity in slice cultures. *Biosens Bioelectron* 1999;14(4):369–76.
- Egert U, Schlosshauer B, Fennrich S, Nisch W, Fejtł M, Knott T, et al. A novel organotypic long-term culture of the rat hippocampus on substrate-integrated multielectrode arrays. *Brain Res Brain Res Protoc* 1998;2(4):229–42.
- Freeman JA, Nicholson C. Experimental optimization of current source-density technique for anuran cerebellum. *J Neurophysiol* 1975;38(2):369–82.
- Gholmieh G, Soussou W, Courellis S, Marmarelis VZ, Berger TW, Baudry M. A biosensor for detecting changes in cognitive processing based on nonlinear systems analysis. *Biosens Bioelectron* 2001;16(7/8):491–501.
- Gholmieh G, Courellis S, Marmarelis VZ, Berger TW. An efficient method for studying short-term plasticity with random impulse train stimuli. *J Neurosci Meth* 2002;121(2):111–27.
- Gholmieh G, Courellis SH, Song D, Wang Z, Marmarelis VZ, Berger TW. Characterization of short-term plasticity of the dentate gyrus-CA3 system using nonlinear systems analysis. In: *Proceedings of the IEEE EMBS conference*; 2003. p. 1929–32.
- Gross GW, Rhoades BK, Reust DL, Schwalm FU. Stimulation of monolayer networks in culture through thin-film indium-tin oxide recording electrodes. *J Neurosci Meth* 1993;50(2):131–43.
- Gross GW, Schwalm FU. A closed flow chamber for long-term multi-channel recording and optical monitoring. *J Neurosci Meth* 1994;52(1):73–85.
- Grumet AE, Wyatt Jr JL, Rizzo III JF. Multi-electrode stimulation and recording in the isolated retina. *J Neurosci Meth* 2000;101(1):31–42.
- Han M, Gholmieh G, Soussou W, Berger TW, Tanguay Jr AR. Conformally-mapped multielectrode arrays for in-vitro stimulation and recording of hippocampal acute slices. In: *Proceedings of the second joint meeting of the IEEE engineering in medicine and biology society and the biomedical engineering society*, vol. 3; 2002. p. 2127–8.
- Heuschkel MO, Fejtł M, Raggenbass M, Bertrand D, Renaud P. A three-dimensional multi-electrode array for multi-site stimulation and recording in acute brain slices. *J Neurosci Meth* 2002;114(2):135–48.
- Hussain RJ, Carpenter DO. The effects of protein kinase C activity on synaptic transmission in two areas of rat hippocampus. *Brain Res* 2003;990(1–2):28–37.
- Jahnsen H, Kristensen BW, Thiebaud P, Noraberg J, Jakobsen B, Bove M, et al. Coupling of organotypic brain slice cultures to silicon-based arrays of electrodes. *Methods* 1999;18(2):160–72.
- Jimbo Y, Robinson HP. Propagation of spontaneous synchronized activity in cortical slice cultures recorded by planar electrode arrays. *Bioelectrochemistry* 2000;51(2):107–15.
- Lanczos C, editor. *Applied Analysis*. Englewood Cliffs, NJ: Prentice-Hall; 1956.
- Leung LS, Fu XW. Factors affecting paired-pulse facilitation in hippocampal CA1 neurons in vitro. *Brain Res* 1994;650(1):75–84.
- McNaughton N, Miller JJ. Medial septal projections to the dentate gyrus of the rat: electrophysiological analysis of distribution and plasticity. *Exp Brain Res* 1984;56(2):243–56.
- Meister M, Pine J, Baylor DA. Multi-neuronal signals from the retina: acquisition and analysis. *J Neurosci Meth* 1994;51(1):95–106.
- Nicholson C, Freeman JA. Theory of current source-density analysis and determination of conductivity tensor for anuran cerebellum. *J Neurophysiol* 1975;38(2):356–68.
- Nicholson C, Llinas R. Real time current source-density analysis using multi-electrode array in cat cerebellum. *Brain Res* 1975;100(2):418–24.
- Novak JL, Wheeler BC. Multisite hippocampal slice recording and stimulation using a 32 element microelectrode array. *J Neurosci Meth* 1988;23(2):149–59.
- Oka H, Shimono K, Ogawa R, Sugihara H, Taketani M. A new planar multielectrode array for extracellular recording: application to hippocampal acute slice. *J Neurosci Meth* 1999;93(1):61–7.
- Pare D, Llinas R. Non-lamellar propagation of entorhinal influences in the hippocampal formation: multiple electrode recordings in the isolated guinea pig brain in vitro. *Hippocampus* 1994;4(4):403–9.
- Richardson TL, Turner RW, Miller JJ. Action-potential discharge in hippocampal CA1 pyramidal neurons: current source-density analysis. *J Neurophysiol* 1987;58(5):981–96.
- Rubinstein JT, Spelman FA, Soma M, Suesserman MF. Current density profiles of surface mounted and recessed electrodes for neural prostheses. *IEEE Trans Biomed Eng* 1987;34(11):864–75.
- Shimono K, Baudry M, Panchenko V, Taketani M. Chronic multichannel recordings from organotypic hippocampal slice cultures: protection from excitotoxic effects of NMDA by non-competitive NMDA antagonists. *J Neurosci Meth* 2002;120(2):193–202.
- Singer W. Why use more than one electrode at a time? In: *New technologies for life sciences: trends guide 2000*; 2000. p. 12–17.
- Soussou W, Gholmieh G, Han M, Ahuja A, Song D, Hsiao M-C, et al. Mapping spatio-temporal electrophysiological activity in hippocampal slices with conformal planar multielectrode arrays. In: Baudry M, Taketani M, editors. *Advances in network electrophysiology using multi electrode arrays*, New York: Kluwer Academic; 2005.
- Steward O. Topographic organization of the projections from the entorhinal area to the hippocampal formation of the rat. *J Comp Neurol* 1976;167(3):285–314.
- Stoppini L, Duport S, Correges P. A new extracellular multirecording system for electrophysiological studies: application to hippocampal organotypic cultures. *J Neurosci Meth* 1997;72(1):23–33.
- Stulik K, Amatore C, Holub K, Marecek M, Kutner W. Microelectrodes. Definitions, characterization, and applications. *Pure Appl Chem* 2000;72(8):1483–92.
- Thiebaud P, de Rooij NF, Koudelka-Hep M, Stoppini L. Microelectrode arrays for electrophysiological monitoring of hippocampal organotypic slice cultures. *IEEE Trans Biomed Eng* 1997;44(11):1159–63.

- Thiebaud P, Beuret C, Koudelka-Hep M, Bove M, Martinoia S, Grattarola M, et al. An array of Pt-tip microelectrodes for extracellular monitoring of activity of brain slices. *Biosens Bioelectron* 1999;14(1):61–5.
- Warland DK, Reinagel P, Meister M. Decoding visual information from a population of retinal ganglion cells. *J Neurophysiol* 1997;78(5):2336–50.
- Wheeler BC, Novak JL. Current source density estimation using microelectrode array data from the hippocampal slice preparation. *IEEE Trans Biomed Eng* 1986;33(12):1204–12.
- Yeckel MF, Berger TW. Feedforward excitation of the hippocampus by afferents from the entorhinal cortex: redefinition of the role of the trisynaptic pathway. *Proc Natl Acad Sci USA* 1990;87(15):5832–6.